An autobias control system for the electro–optic modulator used in a quantum key distribution system*

Chen Wen-Fen(陈文芬), Wei Zheng-Jun(魏正军)†, Guo Li(郭 莉), Hou Li-Yan(侯丽燕), Wang Geng(王 赓), Wang Jin-Dong(王金东), Zhang Zhi-Ming(张智明), Guo Jian-Ping(郭建平), and Liu Song-Hao(刘颂豪)

Laboratory of Nanophotonic Functional Materials and Devices (SIPSE) and Laboratory of Quantum Engineering and Quantum Materials, South China Normal University, Guangzhou 510006, *China*

(Received 14 September 2013; revised manuscript received 25 February 2014; published online 10 June 2014)

In a quantum key distribution system, it is crucial to keep the extinction ratio of the coherent pulses stable. This means that the direct current bias point of the electro–optic modulator (EOM) used for generating coherent pulses must be locked. In this paper, an autobias control system based on a lock-in-amplifier for the EOM is introduced. Its drift information extracting theory and control method are analyzed comprehensively. The long term drift of the extinction ratio of the coherent pulses is measured by a single photon detector, which indicates that the autobias control system is effective for stabilizing the bias point of the EOM.

Keywords: quantum key distribution, electro–optic modulator, autobias control, lock-in-amplifier

PACS: 03.67.Dd, 42.79.Hp, 07.05.Dz **DOI:** 10.1088/1674-1056/23/8/080304

1. Introduction

Since quantum key distribution (QKD) provides an ultimately secure communication based on the laws of quantum mechanics, it has received great attention and different protocols have been proposed. In 1984, Bennett and Brassard presented the first QKD protocol known as the BB84 protocol.[1] In 1992, Bennett presented the protocol using two nonorthogonal states known as B92.[2] In 2003, Inoue *et al.* propounded the protocol differential-phase-shift quantum key distribution (DPS-QKD) using coherent pulses,[3] which has been widely studied for its advantages of communication efficiency[3] and robustness against different attacks.[4] Beside protocols, practical implementation methods of dealing with technical limitations to improve the performance of the QKD system have also been presented.[5–7] In this paper, we pay attention to the technical limitation: the drift of the electro–optic modulator (EOM).

In QKD systems, especially DPS-QKD systems, an EOM is commonly used to convert a continuous-wave (CW) laser beam into pulses to produce coherent pulses, as part of the coherent pulse source.[4,8,9] However, there is a critical problem with the EOM pulsing. The EOM direct current (DC) bias point drifts over time.[10,11] That means that the extinction ratio (ER) of the coherent pulses would decrease with time, causing interference visibility degradation and a higher quantum bit error rate (QBER),[12] and also reducing the QBER margin.

Different methods have been proposed to solve this problem.[13–15] Considering the fact that the CW laser beam in a DPS-QKD system is commonly weak, to measure the EOM drift accurately, the method based on a lock-in-amplifier (LIA) is a good choice for its characteristic of noise compression.[16,17] Nevertheless, the quantitative analysis of its drift information extracting theory has not yet been reported to the best of our knowledge.

In this paper, we make a comprehensive analysis of the autobias control system based on LIA, especially considering the influence of an RF signal, reveal the drift information extracting theory and its application condition, build an autobias control system, apply it to a coherent pulse source, and test its effectiveness through four experiments.

2. Coherent pulse source in the DPS-QKD system

In a DPS-QKD system, when weak coherent pulses that are randomly phase-modulated are sent from a transmitter to a receiver, they are attenuated to less than one photon per pulse on average. To generate coherent pulses, a coherent pulse source is commonly formed by a CW laser and an EOM as shown in Fig. 1.[4,8,9] The EOM converts a CW laser beam into coherent pulses with controllable pulse width and extinction ratio.

*Project supported by the National Natural Science Foundation of China (Grant No. 61108039), the Major Research Plan of the National Natural Science Foundation of China (Grant No. 91121023), and the Scientific Research Foundation of Graduate School of South China Normal University (Grant No. 2012kyjj224).

†Corresponding author. E-mail: weizjweizj@126.com

© 2014 Chinese Physical Society and IOP Publishing Ltd

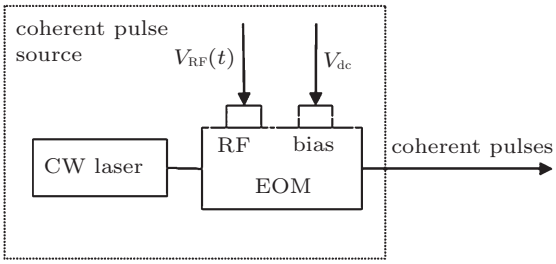


Fig. 1. Schematic diagram of a coherent pulse source.

3. Drift of the electro–optic modulator

An EOM is characterized by taking a cosine function as its transfer function:[18]

$$P_{\text{out}}(t) = \frac{\alpha P_{\text{in}}}{2} + \frac{\alpha P_{\text{in}}}{2} \cos\left\{\frac{\pi}{V_\pi}[V_{\text{DC}} + V_{\text{RF}}(t)] + \theta\right\}, \quad (1)$$

where $P_{\text{out}}(t)$ and P_{in} are the powers of the output light and input light respectively, α is the insertion loss of the EOM, V_π is the half-wave voltage of the EOM, V_{DC} and $V_{\text{RF}}(t)$ are the DC bias voltage and RF modulating signal respectively, and θ is the initial phase of the EOM.

In a DPS-QKD system, the EOM needs to be biased at its minimum point by adjusting the DC bias voltage. However, electrical inhomogeneities or working condition (temperature, humidity, stress) variation of the EOM lead to a drift of the EOM with a change of the initial phase θ in Eq. (1) as a function of time.[10,11,13] Figure 2 shows the drift phenomenon and its influence on the output optical pulses. In the figure, V_{RF} is the RF modulating signal. Over time, the transmission curve drifts from curve 1 to curve 2. The output optical pulses change from pulse 1 to pulse 2, resulting in ER degradation and higher QBER in the DPS-QKD system. So the EOM must be locked.

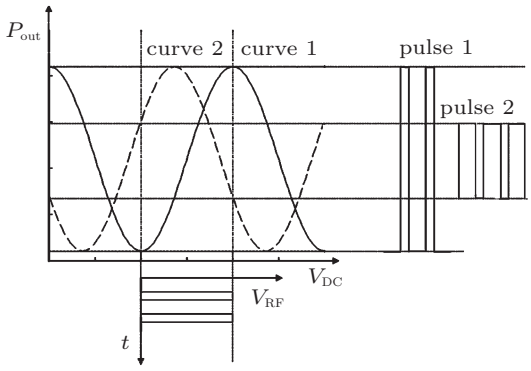


Fig. 2. Drift phenomenon of the EOM.

4. Autobias control system

4.1. Setup

An LIA is capable of extracting the signal at a specific frequency. It outputs a voltage that is proportional to the amplitude of its input signal at the reference frequency and is dependent on the phase difference between the input and reference.[16,19] Therefore, generating a special signal at a particular frequency whose amplitude indicates the drift of an EOM together with an LIA makes it capable of measuring the EOM's drift.

Figure 3 shows an autobias control system based on LIA. It contains a detector, an LIA, a control unit, an adder, and a function generator. The LIA based on AD630 (Anolog Devices) is composed of an amplifier, a phase-sensitive detector (PSD) multiplier, and a low pass filter (LPF). The control unit is comprised of an AT89C51 microcontroller unit (51 MCU), an analog-to-digital converter (ADC), and a digital-to-analog converter (DAC). The autobias control system works as follows.

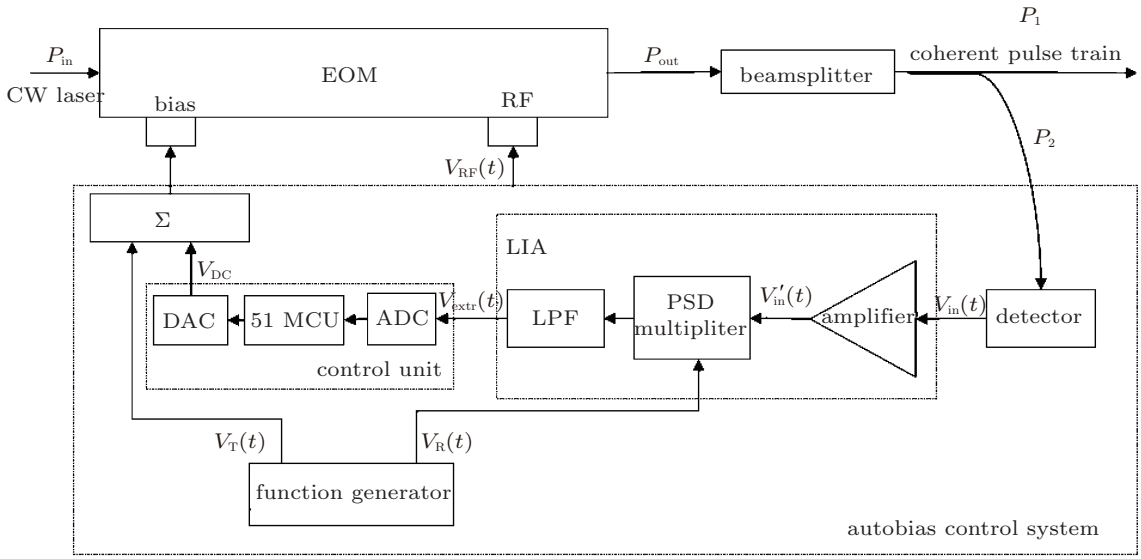


Fig. 3. Schematic diagram of the autobias control system based on LIA.

(i) A function generator: which provides a testing signal ($V_{\rm T}(t)$). It is superimposed on the DC bias voltage and applied to the EOM for carrying out the EOM drift information. $V_{\rm T}(t)$ should be of low amplitude and low frequency so that its influence on the output of the EOM can be ignored.

(ii) A detector: which converts part of the EOM output into an electrical signal ($V_{\rm in}(t)$) for the following circuit.

(iii) A function generator: which provides a reference signal ($V_{\rm R}(t)$). $V_{\rm R}(t)$ has the same frequency and same initial phase as $V_{\rm T}(t)$. It is applied to the LIA for extracting an extracted signal ($V_{\rm extr}(t)$) which carries the EOM drift information from $V_{\rm in}(t)$.

(iv) An ADC: which converts $V_{\rm extr}(t)$ into a digital signal so that it can be read by the 51 MCU. According to the variety of the extracted signal $V_{\rm extr}(t)$, the 51 MCU adjusts its output codes (its control algorithm is described in Subsection 4.3) to drive the DAC generating a DC bias voltage ($V_{\rm DC}$) to the EOM's bias electrode to lock it.

4.2. Drift information extracting theory and control method

In this part, we will describe the process to extract the drift information of the EOM in detail, showing the drift information extracting theory and control method.

According to the discussion in Section 3, the output of the EOM in Fig. 3 can be expressed as

$$P_{\rm out}(t) = \frac{\alpha P_{\rm in}}{2} + \frac{\alpha P_{\rm in}}{2}\cos\left\{\frac{\pi}{V_\pi}[V_{\rm DC} + V_{\rm RF}(t) + V_{\rm T}(t)] + \theta(t)\right\}, \tag{2}$$

since the linearities of the beamsplitter, detector, and amplifier, the input signal of the PSD multiplier can be expressed as a similar expression as follows:

$$V'_{\rm in}(t) = \beta\alpha'\eta G P_{\rm out}(t), \tag{3}$$

where β is the ratio of P_2 to P_1+P_2 (Fig. 3), which is determined by the beamsplitter's splitting ratio, α' is the insertion loss of the beamsplitter, η is the conversion efficiency of the detector, and G is the gain of the amplifier.

The PSD multiplier multiplies its input $V'_{\rm in}(t)$ by the reference signal $V_{\rm R}(t)$. According to trigonometric transformations, we obtain its output signal as follows:

$$\begin{aligned} & y(t) \\ &= AV_{\rm R}(t) + AC\cos\left[\frac{\pi}{V_\pi}V_{\rm DC} + \theta(t)\right]\cos\left[\frac{\pi}{V_\pi}V_{\rm RF}(t)\right]V_{\rm R}(t) \\ &\quad - AC\sin\left[\frac{\pi}{V_\pi}V_{\rm DC} + \theta(t)\right]\sin\left[\frac{\pi}{V_\pi}V_{\rm RF}(t)\right]V_{\rm R}(t) \\ &\quad - AD\sin\left[\frac{\pi}{V_\pi}V_{\rm DC} + \theta(t)\right]\cos\left[\frac{\pi}{V_\pi}V_{\rm RF}(t)\right] \\ &\quad - AD\cos\left[\frac{\pi}{V_\pi}V_{\rm DC} + \theta(t)\right]\sin\left[\frac{\pi}{V_\pi}V_{\rm RF}(t)\right], \end{aligned} \tag{4}$$

where $A = 0.5P_{\rm in}\alpha\beta\alpha'\eta G$, $C = \cos[\pi V_{\rm T}(t)/V_\pi]$, and $D = V_{\rm R}(t)\sin[\pi V_{\rm T}(t)/V_\pi]$.

In this control system, signals $V_{\rm T}(t)$ and $V_{\rm R}(t)$ are square-wave signals with the same frequency, the same initial phase, the same zero mean power, and the same duty ratio of 50%. Based on even and odd qualities of the trigonometric functions, we obtain that C and D are constants.

In a DPS-QKD system, coherent pulses are commonly of a GHz repetition rate and femtosecond width.[20,21] The RF modulating signal of its EOM could be described as

$$\begin{aligned} & V_{\rm RF}(t) = \begin{cases} V_1, & nT_{\rm RF} - T_{\rm w} \le t \le nT_{\rm RF} + T_{\rm w}, \\ V_0, & \text{others}, \end{cases} \\ & n = 0, \pm1, \pm2, \pm3, \ldots, \end{aligned} \tag{5}$$

where $T_{\rm w}$ is half of the pulse width, $T_{\rm RF}$ is the period of $V_{\rm RF}(t)$, and V_0 and V_1 are stable voltages.

According to the laws of Fourier transform, the Fourier transform of $y(t)$ is

$$\begin{aligned} Y(\omega) &= AV'_{\rm R}(\omega) + \frac{AC}{4\pi^2}\times F_1(\omega) * C_{\rm RF}(\omega) * V'_{\rm R}(\omega) \\ &\quad - \frac{AC}{4\pi^2}\times F_2(\omega) * S_{\rm RF}(\omega) * V'_{\rm R}(\omega) \\ &\quad - \frac{AD}{2\pi}\times F_2(\omega) * C_{\rm RF}(\omega) \\ &\quad - \frac{AD}{2\pi}\times F_1(\omega) * S_{\rm RF}(\omega), \end{aligned} \tag{6}$$

where $V'_{\rm R}(\omega)$, $F_1(\omega)$, $F_2(\omega)$, $C_{\rm RF}(\omega)$, $S_{\rm RF}(\omega)$ are the Fourier transforms of $V_{\rm R}(t)$, $\cos[(\pi/V_\pi)V_{\rm DC} + \theta(t)]$, $\sin[(\pi/V_\pi)V_{\rm DC} + \theta(t)$, $\cos[(\pi/V_\pi)V_{\rm RF}(t)$, $\sin[(\pi/V_\pi)V_{\rm RF}(t)]$ respectively.

The components of $Y(\omega)$ are listed in Table 1.[22]

Because the drift of the EOM is slow, $F_1(\omega)$ is not zero only within a small range of low frequency, neither is $F_2(\omega)$. Because $V_{\rm RF}(t)$ is of a high frequency, the value of $\omega_{\rm RF}$ is much larger than $\omega_{\rm R}$. Therefore, components 1, 2, 4, 7, and 9 will be eliminated by the LPF, if the following inequalities hold:

$$\begin{cases} \omega_{\rm R} \ge 2\cdot\max\{\omega_{\rm dCO}, \omega_{\rm dSI}\}, \\ \max\{\omega_{\rm dCO}, \omega_{\rm dSI}\} \le \omega_{\rm db} \le \omega_{\rm R} - \max\{\omega_{\rm dCO}, \omega_{\rm dSI}\}, \end{cases} \tag{7}$$

where $\omega_{\rm dCO}$ and $\omega_{\rm dSI}$ are the cut-off angular frequencies of $F_1(\omega)$ and $F_2(\omega)$, $\omega_{\rm R}$ is the angular frequency of $V_{\rm R}(t)$, and $\omega_{\rm db}$ is the bandwidth of the LPF.

For component 3, only the items which meet $|m\omega_{\rm R} + k\omega_{\rm RF}| \le \omega_{\rm db} + \omega_{\rm dCO}$ could pass through the LPF. Owing to the huge value of $\omega_{\rm RF}$ and the low value of $\omega_{\rm R}$, these items have m of huge value and negligible amplitude. They could be neglected. Component 5 is of the same situation.

The angular frequencies of component 6 and component 8 are lower than $\omega_{\rm db}$. So, the output of the LPF is

Table 1. Components of $Y(\omega)$.

Components of $Y(\omega)$		No.
Expression	Detail	
$AV'_{\rm R}(\omega)$	$AA_{\rm R}\sum_{k\neq0}\frac{2\sin 0.5k\pi}{k\pi}2\pi\delta(\omega-k\omega_{\rm R})$	1
$\frac{AC}{4\pi^2}\times F_1(\omega)*C_{\rm RF}(\omega)*V'_{\rm R}(\omega)$	$ACA_{\rm R}\cos\left(\frac{\pi V_0}{V_\pi}\right)F_1(\omega)*\sum_{k\neq0}\frac{2\sin 0.5k\pi}{k\pi}\delta(\omega-k\omega_{\rm R})$	2
	$+ACA_{\rm R}\left[\cos\left(\frac{\pi V_1}{V_\pi}\right)-\cos\left(\frac{\pi V_0}{V_\pi}\right)\right]F_1(\omega)*\sum_k\sum_{m\neq0}\frac{\sin k\omega_{\rm RF}T_{\rm w}}{k\pi}\frac{2\sin 0.5m\pi}{m\pi}\delta(\omega-m\omega_{\rm R}-k\omega_{\rm RF})$	3
$-\frac{AC}{4\pi^2}\times F_2(\omega)*S_{\rm RF}(\omega)*V'_{\rm R}(\omega)$	$-ACA_{\rm R}\sin\left(\frac{\pi V_0}{V_\pi}\right)F_2(\omega)*\sum_{k\neq0}\frac{2\sin 0.5k\pi}{k\pi}\delta(\omega-k\omega_{\rm R})$	4
	$-ACA_{\rm R}\left[\sin\left(\frac{\pi V_1}{V_\pi}\right)-\sin\left(\frac{\pi V_0}{V_\pi}\right)\right]F_2(\omega)*\sum_k\sum_{m\neq0}\frac{\sin k\omega_{\rm RF}T_{\rm w}}{k\pi}\frac{2\sin 0.5m\pi}{m\pi}\delta(\omega-m\omega_{\rm R}-k\omega_{\rm RF})$	5
$-\frac{AD}{2\pi}\times F_2(\omega)*C_{\rm RF}(\omega)$	$-AD\left[\left(1-\frac{2T_{\rm w}}{T_{\rm RF}}\right)\cos\left(\frac{\pi V_0}{V_\pi}\right)+\frac{2T_{\rm w}}{T_{\rm RF}}\cos\frac{\pi V_1}{V_\pi}\right]F_2(\omega)$	6
	$-AD\sum_{k\neq0}\left(\cos\frac{\pi V_1}{V_\pi}-\cos\frac{\pi V_0}{V_\pi}\right)\frac{\sin k\omega_{\rm RF}T_{\rm w}}{k\pi}F_2(\omega-k\omega_{\rm RF})$	7
$-\frac{AD}{2\pi}\times F_1(\omega)*S_{\rm RF}(\omega)$	$-AD\left[\left(1-\frac{2T_{\rm w}}{T_{\rm RF}}\right)\sin\left(\frac{\pi V_0}{V_\pi}\right)+\frac{2T_{\rm w}}{T_{\rm RF}}\sin\frac{\pi V_1}{V_\pi}\right]F_1(\omega)$	8
	$-AD\sum_{k\neq0}\left(\sin\frac{\pi V_1}{V_\pi}-\sin\frac{\pi V_0}{V_\pi}\right)\frac{\sin k\omega_{\rm RF}T_{\rm w}}{k\pi}F_1(\omega-k\omega_{\rm RF})$	9

$\omega_{\rm R}$ is the angular frequency of $V_{\rm R}(t)$. $A_{\rm R}$ is the amplitude of $V_{\rm R}(t)$. $\omega_{\rm RF}$ is the angular frequency of $V_{\rm RF}(t)$.

$$\begin{aligned}V_{\rm extr}(t) &= -AD\left[\left(1-\frac{2T_{\rm w}}{T_{\rm RF}}\right)\cos\frac{\pi V_0}{V_\pi}+\frac{2T_{\rm w}}{T_{\rm RF}}\cos\frac{\pi V_1}{V_\pi}\right]\\&\quad\times\sin\left[\frac{\pi V_{\rm DC}}{V_\pi}+\theta(t)\right]\\&\quad-AD\left[\left(1-\frac{2T_{\rm w}}{T_{\rm RF}}\right)\sin\frac{\pi V_0}{V_\pi}+\frac{2T_{\rm w}}{T_{\rm RF}}\sin\frac{\pi V_1}{V_\pi}\right]\\&\quad\times\cos\left[\frac{\pi V_{\rm DC}}{V_\pi}+\theta(t)\right].\end{aligned}\tag{8}$$

According to trigonometric transformations, equation (8) turns into

$$V_{\rm extr}(t)=-ADH\sin\left[\Phi+\frac{\pi V_{\rm DC}}{V_\pi}+\theta(t)\right],\tag{9}$$

where

$$\begin{aligned}H &= \left\{\left[\left(1-\frac{2T_{\rm w}}{T_{\rm RF}}\right)\cos\frac{\pi V_0}{V_\pi}+\frac{2T_{\rm w}}{T_{\rm RF}}\cos\frac{\pi V_1}{V_\pi}\right]^2\right.\\&\quad\left.+\left[\left(1-\frac{2T_{\rm w}}{T_{\rm RF}}\right)\sin\frac{\pi V_0}{V_\pi}+\frac{2T_{\rm w}}{T_{\rm RF}}\sin\frac{\pi V_1}{V_\pi}\right]^2\right\}^{1/2}\\&=\sqrt{1+2\frac{2T_{\rm w}}{T_{\rm RF}}\left(1-\frac{2T_{\rm w}}{T_{\rm RF}}\right)\left(\cos\frac{\pi(V_1-V_0)}{V_\pi}-1\right)},\end{aligned}\tag{10}$$

$$\Phi=\arctan\frac{\left[\left(1-\frac{2T_{\rm w}}{T_{\rm RF}}\right)\sin\frac{\pi V_0}{V_\pi}+\frac{2T_{\rm w}}{T_{\rm RF}}\sin\frac{\pi V_1}{V_\pi}\right]}{\left[\left(1-\frac{2T_{\rm w}}{T_{\rm RF}}\right)\cos\frac{\pi V_0}{V_\pi}+\frac{2T_{\rm w}}{T_{\rm RF}}\cos\frac{\pi V_1}{V_\pi}\right]}.\tag{11}$$

According to Eq. (9), the voltages and duty ratio of the RF modulating signal $V_{\rm RF}(t)$ influence the amplitude and phase of $V_{\rm extr}(t)$.

According to Eq. (10), if the mean values of $\cos(\pi V_{\rm RF}(t)/V_\pi)$ and $\sin(\pi V_{\rm RF}(t)/V_\pi)$ are zero at the same time, "H" will be identically zero and $V_{\rm extr}(t)$ also becomes identically zero. This will cause the autobias control system to be invalid. Hence for using this autobias control system effectively, "H" must not be zero, which means that the mean values of $\cos(\pi V_{\rm RF}(t)/V_\pi)$ and $\sin(\pi V_{\rm RF}(t)/V_\pi)$ should not be zero at the same time.

If "H" is not zero, $V_{\rm extr}(t)$ is a function of $\theta(t)$ and $V_{\rm DC}$. The autobias control unit could lock the EOM by adjusting the DC bias voltage to counteract the drift of $\theta(t)$ according to the variety of $V_{\rm extr}(t)$. Hence this autobias control system is appropriate for the systems in which "H" is not zero.

The DPS-QKD system is a typical example of applying this autobias control system, because it employs electrical pulses of duty ratio much less than 50% and the peak-to-peak value of $|V_1-V_0|=V_\pi$ to drive the EOM to generate coherent pulses. According to trigonometric transformations, after applying $|V_1-V_0|=V_\pi$ in Eq. (9) the resulting expression turns into

$$\begin{aligned}&V_{\rm extr}(t)\\&=-AD\left(1-\frac{4T_{\rm w}}{T_{\rm RF}}\right)\sin\left(\frac{\pi V_0}{V_\pi}+\frac{\pi V_{\rm DC}}{V_\pi}+\theta(t)\right).\end{aligned}\tag{12}$$

4.3. Control algorithm

The control algorithm of the control unit is described as follows.

i) Find the EOM minimum point

When the EOM works without an RF modulating signal, V_0 and V_1 in Eq. (8) will be zero and the resulting Eq. (8) turns into

$$V_{\text{extr}}(t) = -AD\sin\left[\theta(t) + \frac{\pi V_{\text{DC}}}{V_\pi}\right]. \tag{13}$$

Meanwhile, to bias the EOM at its minimum point, $\theta(t) + \pi V_{\text{DC}}/V_\pi$ should be $\pi + 2k\pi$ ($k = 0, \pm1, \pm2, \pm3$) according to the EOM's transfer function Eq. (1). Thus, the zero points with a negative slope in the relation curve of V_{DC} and $V_{\text{extr}}(t)$ (as described in Eq. (13)) indicate that the EOM is biased at its minimum point, if $D < 0$ (when the amplifier is an inverting amplifier).

Therefore, without applying the RF signal to the EOM, scan $V_{\text{extr}}(t)$ by increasing the output (V_{DC}) of the control unit step by step until the minimum point of the EOM is found.

ii) Store the value of $V_{\text{extr}}(t)$, with the RF applied to the EOM.

After finding the minimum point of the EOM maintain the value of V_{DC}, apply the RF modulating signal $V_{\text{extr}}(t)$ immediately, read the value of $V_{\text{extr}}(t)$ and store it in a memory.

iii) Lock the EOM

Constantly read $V_{\text{extr}}(t)$, compare it with the value stored, adjust V_{DC} once the read and stored values are unequal. If the read $V_{\text{extr}}(t)$ value is larger than the value stored, increase V_{DC}; otherwise, reduce V_{DC}.

5. Experiments and results

In this section, a coherent pulse source with an autobias control system based on LIA is built. The setup scheme for testing its performance is shown in Fig. 4. Firstly, an InGaAsP diode laser which delivers a 1550-nm laser is employed as the CW laser. Then, a polarization controller (PC) (SFFPC010, Shenzhen Shinemits Technology Limited) is used for better coupling the CW laser output into the EOM (SMS-55-SS-SP, Shenzhen Shinemits Technology Limited). Then the beamsplitter (WBC-22-135-50-1-09-FC/PC-B, WRI) splits the output of the EOM into two: one for the autobias control system and the other for testing. The variable attenuator (FVA 3100, EXFO) attenuates one of the beamsplitter outputs to ensure that the input of the single photon detector is less than 0.1 photon per gate on average. The single photon detector (id-201 SPDM, IDQ) measures the output of the variable attenuator. The digital delay generator (DG535, SRS) is used to synchronize the trigger signal of the single photon detector with its input optical pulse train. The RF signal generator designed by our laboratory provides synchronization signals: the RF modulating signal $V_{\text{RF}}(t)$ for the EOM and the trigger signal $V_{\text{Tri}}(t)$ for the single photon detector. The fibers connecting the different apparatuses are single-mode fibers.

Since the EOM is polarization-dependent, for excluding the drift of the EOM's input light from the experimental results, its power and polarization states are monitored long term by the setup shown in Fig. 5. The PC controls the polarization state of the CW laser output. The beamsplitter splits the output of the PC into two parts: one is for power testing and the other is for polarization state testing. The types of the PC and the beamspliter are the same as those in Fig. 4 respectively.

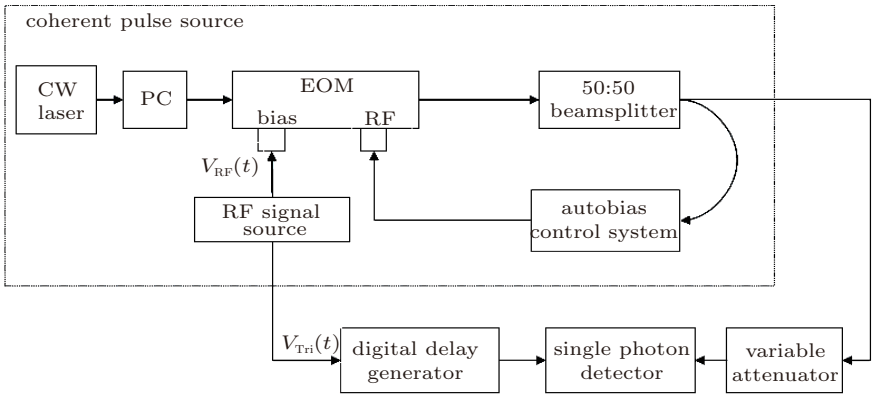


Fig. 4. Setup scheme for testing the performance of the autobias control system.

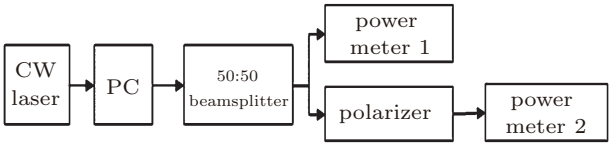


Fig. 5. Setup for stabilization test of the CW laser.

According to the Stokes vector, the degree of polarization (DOP) and polarizing angle (α) of a light can be obtained from the following expression:[23]

$$\text{DOP} = \frac{\sqrt{(I_0 - I_{90})^2 + (I_{45} - I_{135})^2}}{I_0 + I_{90}},$$

$$\alpha = 0.5 \arctan \frac{I_{45} - I_{135}}{I_0 - I_{90}}, \tag{14}$$

where I_0, I_{45}, I_{90}, and I_{135} are the intensities of the light in the polarizing directions of 0°, 45°, 90°, 135° respectively.

Firstly, set the CW laser output power to be some value. In this experiment, it is set to make power meter 1 (XR1882, XIRON) receive a light of 56.585 μW. Then note the values of power meter 2 (PM-1600, EXPO) when the direction of the transmission axis of the polarizer is located at angels of 0°, 45°, 90°, 135°, and note the value of power meter 1 every 15 min for 7 h. During the experiment, the fibers between different apparatuses are kept still and the room temperature is kept between 19 °C and 22 °C. The results are shown in Figs. 6 and 7.

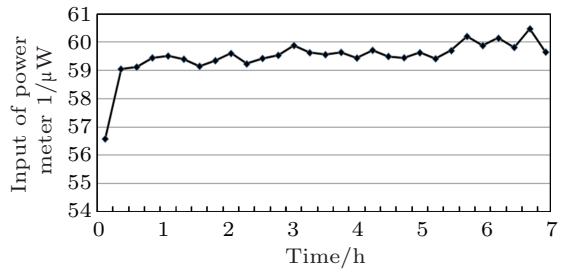


Fig. 6. Evolution of the power meter 1 input.

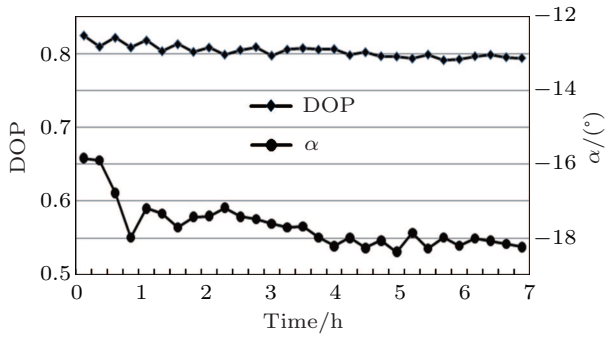


Fig. 7. Evolution of the CW laser polarization state.

As shown in Fig. 6, the input light of power meter 1 has a drift of 2.471 μW at the first 15 min. Then it fluctuates between 59.056 μW and 60.478 μW. As shown in Fig. 7, α has a drift of −2.15° at the first 45 min. Then it fluctuates between −18.37° and −17.18°. The DOP fluctuates between 7.91 and 8.25 in 7 h. The drift of α and the fluctuation of DOP may be due to a small change of the room temperature, the birefringence effect of the fibers, a recovery of the fibers after being strained or just an error due to the error in locating the polarizer at different angles each time. These results suggest that after the CW laser works for 45 min, the input light of the EOM in Fig. 4 would be more stable and the drift of the input light of the EOM can be excluded from the experimental results.

For testing the performance of the autobias control system, we measure the drift of the pulse base and the drift of ER of the coherent pulse source when the EOM works without or with the autobias control system. Here the pulse base is the output of the coherent pulse source, when the EOM works without the RF modulating signal and is biased at its minimum point. In these experiments, the CW laser has been working for more than 45 min before testing. The fibers between different apparatuses are kept still and the room temperature is kept between 19 °C and 22 °C during these experiments. All these are done to exclude the drift of the input light of the EOM from the testing results and ensure that a similar working condition of the EOM is maintained during the testing.

In the first experiment, the pulse base drift of the coherent pulse source is measured when the EOM works without bias control. Since the linear relationship between the coherent pulse source output and the single photon detector input, the pulse base drift of the coherent pulse source can be measured by monitoring the drift of the photon counting of the single photon detector, when the average photon number per gate is less than 0.1.[24] The experiment is carried out as follows. Firstly, the RF modulating signal $V_{\mathrm{RF}}(t)$ in Fig. 4 is turned off. The power of the input light of the EOM is set to be 101.81 μW. The single photon detector works with a 2.5-ns gate width and 107142.6-Hz trigger frequency. Its dead time is set to be invalid. Its dark counting (C_{dark}) is 2.18 Hz. Then the EOM is biased at its minimum point by a DC bias voltage. It is kept during the experiment. The photon counting of single photon detector (C_{photo}) is noted every 15 min for 7 h. The result is shown as line 1 in Fig. 8.

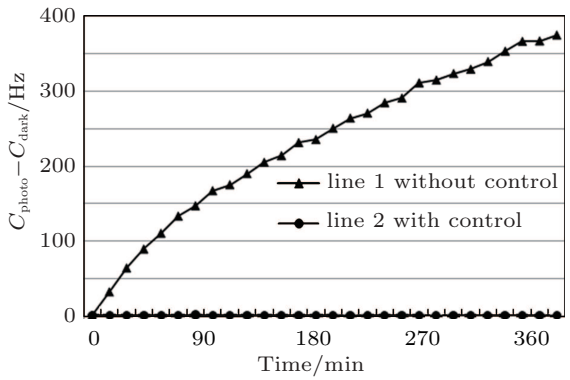


Fig. 8. Comparison of the pulse base evolution of the coherent pulse source between without (line 1) and with (line 2) bias control.

In the second experiment, the pulse base drift of the coherent pulse source is measured when the EOM works with the autobias control system. For ensuring the comparability of the results between the first experiment and the second experiment, the second experiment is done exactly in the same manner as the first one, except the EOM works with the autobias control system. The result is shown as line 2 in Fig. 8.

According to Fig. 8, without bias control, the pulse base of the coherent pulse source has an evident drift. $C_{\text{photo}} - C_{\text{dark}}$ drifts from 1.51 Hz to 599.08 Hz. Since the stabilization of the input light of the EOM has been proved above, this drift is mainly due to the drift of the EOM. Working condition variation or electrical inhomogeneities of the EOM could cause its drift. Since the working condition in this experiment is kept similar, the drift is mainly due to the electrical inhomogeneities. Electrical inhomogeneities of the EOM cause a redistribution of the electrical charge, yielding the occurrence of a time-dependent depolarizing electric field, when a bias voltage is applied.[13] That means that there will be an unstable inner field if the DC bias voltage keeps still. In other words, the voltage is actually used to modulate the input light changes over time, leading to a change of the phase θ in Eq. (1). Thus, the pulse base of the coherent pulse source drifts. Working with the autobias control system, the pulse base of the coherent pulse source fluctuates within a small range. The EOM is locked around its minimum point. $C_{\text{photo}} - C_{\text{dark}}$ is kept between 0.79 Hz and 1.44 Hz. That is because the autobias control system adjusts the DC bias voltage to compensate for the changing of the inner electric field, thereby maintaining the actually modulating voltage.

In the third experiment, the ER drift of the coherent pulse source is evaluated when the EOM works with an RF modulating signal and without control. According to the linear relationship mentioned in the first experiment, the ER of the output of the coherent pulse source can be gained from the following expression:

$$\text{ER} = 10 \lg \frac{N - C_{\text{dark}}}{M - C_{\text{dark}}}, \tag{15}$$

where N and M are the photon countings of the single photon detector, which relate to the pulse top and the base of the coherent pulse respectively.

Therefore, we can evaluate the ER drift by monitoring the values of N and M. The power of the EOM input light is set to be 102.78 μW. The EOM is biased at its minimum point and the DC bias voltage is kept still. An RF modulating signal $V_{\text{RF}}(t)$ with a 2.2-V amplitude and 704-ps pulse width is applied to the EOM. The single photon detector works in the same manner as that in the first two experiments. Every 15 min, we adjust the delay time of the digital delay generator to synchronize the single photon detector with the pulse top and the base of the coherent pulse, recording the values of N and M respectively. The drift of the ER gained from M and N is shown as line 1 in Fig. 9.

In the fourth experiment, the ER drift of the coherent pulse source is evaluated when the EOM works with an RF modulating signal and with the autocontrol system. For ensuring the comparability between the results in the third experiment and those in the fourth experiment, the input light of the EOM, the RF modulating signal and the single photon detector work in the same manner as those in the third experiment. N and M are recorded every 15 min for 7 h. The result is shown as line 2 in Fig. 9.

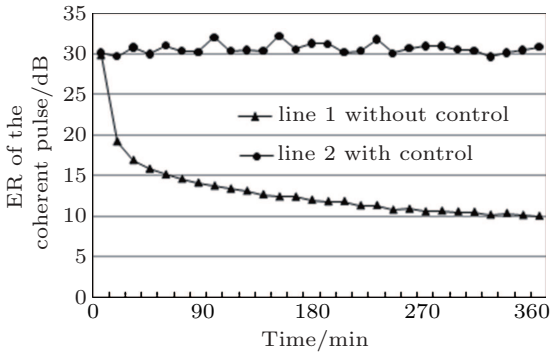


Fig. 9. Comparison of the ER evolution of the coherent pulse source between without (line 1) and with (line 2) bias control.

As shown in Fig. 9, without bias control, the ER changes from 29.87 dB to 9.97 dB in 7 h. That is because the drift of θ (referring to the first experiment) degrades the ER, as explained in Section 3. While working with the autocontrol system, it is kept between 29.64 dB and 32.18 dB. The unstable inner field due to electrical inhomogeneities is compensated by the autobias control system. The ER remains still.

The experiments indicate that by using the autobias control system presented in this paper, the EOM is locked and the output of the coherent pulse source is stabilized.

6. Conclusion

In this paper, we present an autobias control system based on LIA. The comprehensive analysis of the process to extract the drift information verifies the feasibility of this drift measurement and control method. The relationship between the extracted signal and the RF modulating signal is obtained, and so are the application conditions of the autobias control system. This autobias control system is applied to the EOM used in a coherent pulse source. Experiments show that the EOM is locked and the ER of the coherent pulses is kept between 29.64 dB and 32.18 dB in 7 h.

References

[1] Bennett C H and Brassard G 1984 *Proceedings of the IEEE International Conference on Computers, Systems, and Signal Processing*, December 9–12, 1984, Bangalore, India, p. 175
[2] Bennett C H 1992 *Phys. Rev. Lett.* **68** 3121
[3] Inoue K, Waks E and Yamamoto Y 2003 *Phys. Rev. A* **68** 022317
[4] Takesue H, Diamanti E, Honjo T, Langrock C, Fejer M M, Inoue K and Yamamoto Y 2005 *New J. Phys.* **7** 232
[5] Zhou Y Y, Zhou X J, Tian P G and Wang Y J 2013 *Chin. Phys. B* **22** 010305
[6] Zhang Y, Wang S, Yin Z Q, Chen W, Liang W Y, Li H W, Guo G C and Han Z F 2012 *Chin. Phys. B* **21** 100307
[7] Wang J D, Qin X J, Wei Z J, Liu X B, Liao C J and Liu S H 2010 *Acta Phys. Sin.* **59** 281 (in Chinese)
[8] Takesue H , Honjo T, Tamaki K and Tokura Y 2009 *IEEE Commun. Mag.* **47** 102

[9] Inoue K, Ohashi T, Kukita T, Watanabe K, Hayashi S, Honjo T and Takesue H 2008 *Opt. Express* **16** 15469

[10] Salvestrini J P, Guilbert L, Fontana M, Abarkan M and Gille S 2011 *J. Lightwave Technol.* **29** 1522

[11] Bui D T, Nguyen L D, Ledoux-Rak I and Journet B 2010 *Optical Components and Materials VI*, January 26–28, 2010, San Francisco, UAS, p. 75980R

[12] Nicolas G, Gregoire R, Wolfgang T and Hugo Z 2002 *Rev. Mod. Phys.* **74** 145

[13] Bui D T, Pham T T, Vu V Y and Journet B 2012 *4th International Conference on Communications and Electronics (ICCE)*, August 1–3, 2012, Hue, Vietnam, p. 63

[14] Bui D T, Nguyen C T, Ledoux-Rak I, Zyss J and Journet B 2011 *Meas. Sci. Technol.* **22** 125105

[15] Huang Z J, Zhang X M, Zheng S L, Jin X F and Chi H 2011 2011 *IEEE International Topical Meeting on Microwave Photonics,* October 18–21, 2011, Singapore, Singapore, p. 218

[16] Snoddy J, Li Y, Ravet F and Bao X Y 2007 *Appl. Opt.* **46** 1482

[17] Wada Y, Taketomi A, Inoue T, Hashimo M, Kamba Y, Matsuura J, Tei K, Yamaguchi S, Enokidani J and Sumida S 2011 2011 *International Quantum Electronics Conference (IQEC) and Conference on Lasers and Electro-Optics (CLEO) Pacific Rim,* August 28–September 1, 2011, Sydney, Australia, p. 1730

[18] Chen Y N, Zhang X Q and Li D 2009 *9th International Conference on Electronic Measurement & Instruments (ICEMI* 2009*)*, August 16–19, 2009, Beijing, China, pp. 3–950

[19] Gao J Z 2004 *Detection of Weak Signals* (Beijing: Tsinghua University Press) p. 154 (in Chinese)

[20] Inoue K and Honjo T 2005 *Phys. Rev. A* **71** 042305

[21] Ma L, Nam S, Xu H, Baek B, Chang T, Slattery O, Mink A and Tang X 2009 *New J. Phys.* **11** 045020

[22] Oppenheim A V, Willskey A S and Nawmid S 1999 *Signals & Systems*, 2nd edn. (Beijing: Tsinghua University Press) p. 202 (in Chinese)

[23] Wang Z, Hong J, Qiao Y L, Wang F and Yang W F 2007 *Optical Technique* **33** 196 (in Chinese)

[24] Liu J F, Liang R S, Liu W P, Tang Z L, Zheng L M, Wei Z J, Chen Z X, Liao C J and Liu S H 2004 *Acta Photonica Sin.* **33** 867 (in Chinese)